8 Processing and Deformation Characteristics of Metals Reinforced with Ceramic Nanoparticles

Sie Chin Tjong[1,2]

[1]Department of Physics and Materials Science, City University of Hong Kong, Tat Chee Avenue, Kowloon, Hong Kong, PR China, [2]Department of Physics, Faculty of Science, King Abdulaziz University, Jeddah, Saudi Arabia

8.1 Introduction

Metal matrix composites (MMCs) reinforced with continuous ceramic fibers exhibit high specific strength and specific elastic modulus over unreinforced metals/alloys [1]. The high cost of reinforcing fibers and high processing cost of fiber-reinforced MMCs render them uneconomical for technological applications. In contrast, MMCs reinforced with ceramic microparticles are isotropic, easier to manufacture, and lower cost in comparison to the continuous fiber-reinforced composites. MMCs inherent excellent properties from their matrix alloy and the reinforcing phase components, i.e., ductility and toughness of the metal matrix, high modulus and strength of the reinforcement. Therefore, particulate-reinforced MMCs exhibit high strength, superior creep, and wear resistances [2–6]. They find a broad range of applications from structural components in the aerospace, automotive, and transportation industries to the thermal management for electronic devices [7,8]. Generally, the metal matrices used in the particulate-reinforced MMCs include commercially available alloys based on aluminum, magnesium, and titanium. Among them, aluminum-based alloys with face-centered cubic structure are used extensively due to their low density, good workability, and tailored mechanical property. The mechanical strength of heat-treatable aluminum alloys can be increased dramatically through aging heat treatment due to the formation of fine precipitates, i.e., precipitation hardening. However, precipitation-hardened aluminum alloys suffer a large reduction in mechanical strength upon exposure to elevated temperature for long periods because of the precipitate coarsening. Ceramic particles are stable at temperatures up to the melting temperature of the matrix metal and do not coarsen at elevated temperatures.

Particulate-reinforced MMCs generally contain large volume fraction of reinforcement to achieve desired mechanical and physical properties. High reinforcement

Nanocrystalline Materials. DOI: http://dx.doi.org/10.1016/B978-0-12-407796-6.00008-7

loadings impair mechanical properties and increase the weight of resulting composites. Furthermore, ceramic particles with sizes of several micrometers often act as the preferential sites for crack initiation and propagation, resulting in low mechanical ductility and toughness. In recent years, the escalation cost of fossil fuel and the urgent need of reducing carbon dioxide emission have driven materials scientists to search for light-weight structural materials for use in aerospace and transportation industries.

With the advent of nanotechnology, novel nanocrystalline materials with unique chemical, physical, and mechanical properties have been developed and synthesized recently. Nanocrystalline materials exhibit much higher mechanical strength and modulus compared to their microcrystalline counterparts. Inorganic nanoparticles can be synthesized from a wide variety of techniques, including sol−gel, spray forming, chemical vapor deposition, and laser-induced gas phase reaction [9]. Thus, ceramic nanomaterials overcome the limitations of microcrystalline counterparts, showing great potential for use as reinforcing components for metals. For example, Tjong and coworkers introduced silicon nitride nanoparticles (10 nm) to the aluminum matrix, and reported that the tensile strength 1 vol% Si_3N_4/Al nanocomposite is comparable to that of 15 vol% SiC (3.5 μm)/Al microcomposite. The yield stress of 1 vol% Si_3N_4/Al nanocomposite is significantly higher than that of the 15 vol% SiC-reinforced microcomposite [10]. Furthermore, the additions of 1−2 vol% Si_3N_4 nanoparticles to aluminum also enhance its high-temperature creep resistance markedly [11].

In spite of several advantages of reinforcing ceramic nanoparticles, the fabrication of metal matrix nanocomposites (MMNCs) remains a big challenge for materials scientists. Ceramic nanoparticles of large surface areas often agglomerate into clusters since they are poorly wetted with metals during the composite fabrication. In this regard, several processing strategies have been adopted to fabricate MMNCs with homogeneous dispersion of nanoparticles in the metal matrix. These include compocasting, ultrasonic cavitation, ball milling, and friction stir processing (FSP). The microstructures and mechanical properties of MMNCs depend greatly on the processing technique employed. This chapter overviews the state-of-the-art development in the processing strategies and mechanical deformation characterization of MMNCs reinforced with ceramic nanoparticles. Particular attention is paid to their structure−property relationships.

8.2 Fabrication of MMNCs

Two processing routes are generally deployed for fabricating MMNCs, i.e., liquid- and solid-state processing. Liquid-state processing route includes melt stirring and compocasting. Liquid-state processing is widely known to be very cost-effective since it can produce bulk composites in large quantities using existing melting and casting facilities. However, particle agglomeration, poor wetting of ceramic nanoparticles with molten metal, and preferential formation of interfacial products

hinder its extensive use for manufacturing MMNCs. The potential of bulk MMNCs cannot be fully realized for industrial applications unless nanocomposite structural components can be manufactured cost effectively using liquid-state processing route. Because of poor wettability between the metal matrix and ceramic particles, the reinforcing particulates tend to agglomerate into clusters in the matrix. Therefore, an external force field is required to break up the clusters and disperse them into the melt. This can be done by using high intensity ultrasonic probe for creating violent agitation in the melt, terming as the ultrasonic cavitation [12–15].

Solid-state processing route is typically a powder metallurgy (PM)-based process, in which the matrix powder and reinforcing materials are mixed together in a simple mechanical mixer followed by cold compaction and sintering, hot pressing, or spark plasma sintering (SPS) to form a bulk composite. Conventional furnace sintering requires high temperature and long heating time to obtain dense products. In contrast, SPS offers advantages of low processing temperature and very short heating time for consolidating composite powders. In certain cases, secondary mechanical processing such as hot extrusion, hot forging, hot rolling, or FSP is necessary to further improve mechanical properties of MMNCs by consolidating the compacts into full-dense products. PM processing has the advantages of better dispersion of reinforcing particles and near net-shape fabrication. The disadvantage is the high cost of powder materials.

8.2.1 Liquid-State Processing

Depending on the temperature at which the reinforcing particles are introduced into the melt, there exist two types of melting practices for fabricating composites. In the stir mixing/casting process, the particles are added to molten alloy above its liquidus temperature. On the contrary, ceramic nanoparticles are introduced into metal in the semisolid state in the compocasting process. Stir casting involves an initial melting of metal/alloy ingots in a furnace in a protective gas atmosphere, mixing nanoparticles with molten metal using an impeller followed by solidification. In this process, both the incorporation of nanoparticles into the melt and pouring of the composite slurry into the mould are carried out in a fully liquid state. Figure 8.1 is a schematic diagram showing a typical setup commonly used for manufacturing MMNCs using melt stirring [16]. A graphite impeller stirs a melt mixture vigorously, generating a vortex in the melt for dispersing nanoparticles. The main drawbacks of stir casting are poor wettability between molten metal and ceramic nanoparticles, and high-porosity content of the composite products. Moreover, reinforcing particles tend to float or sink depending on their density relative to the liquid metal. These issues become especially significant as the reinforcement size decreases due to greater agglomeration tendency and reduced wettability of the particles with the melt (Figure 8.2) [17].

The wetting of a solid surface with molten metal plays an important role in the dispersion of ceramic nanoparticle in the metal matrix. Wetting relates to the contact between a liquid and a solid surface, describing the ability of a liquid to spread

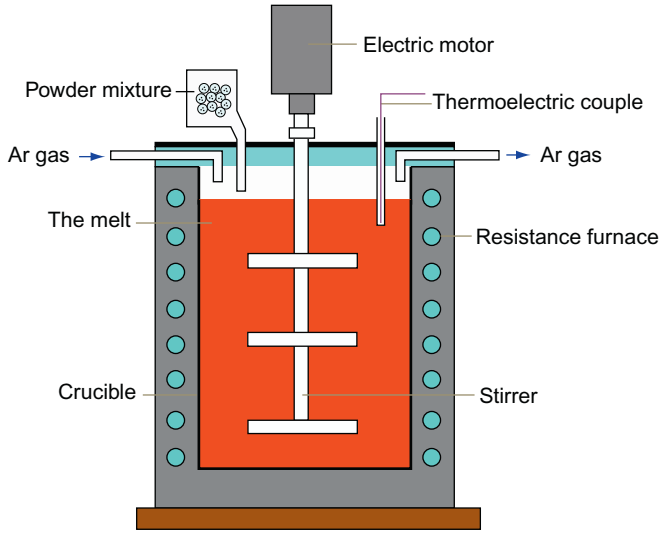

Figure 8.1 Setup for stir casting.
Source: Reprinted from Ref. [16] with permission of Elsevier.

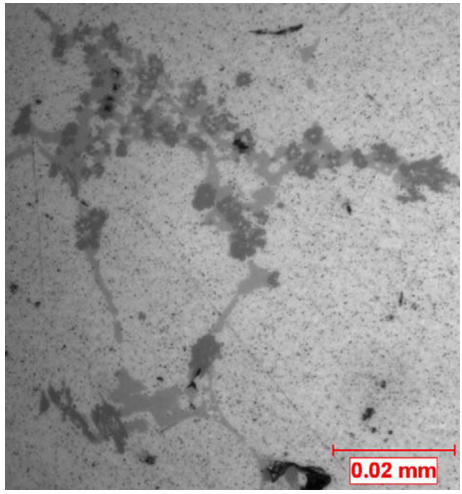

Figure 8.2 Agglomeration of alumina nanoparticles (47 nm) at the grain boundaries of 5 wt% Al_2O_{3p}/A206 nanocomposite.
Source: Reprinted from Ref. [17] with permission of Elsevier.

over a solid surface by minimizing surface free energy. For a liquid droplet on a solid surface (Figure 8.3), the surface energy (tension) of different components can be expressed by

$$\gamma_{SV} = \gamma_{SL} + \gamma_{LV} \cos \phi \tag{8.1}$$

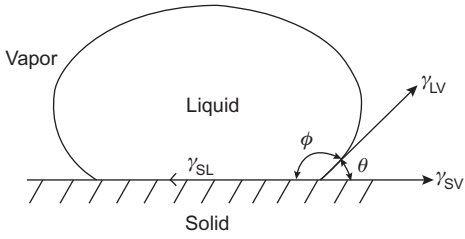

Figure 8.3 Schematic diagram showing a liquid droplet on a solid.

$$\cos\phi = \frac{\gamma_{SV} - \gamma_{SL}}{\gamma_{LV}} \tag{8.2}$$

where ϕ is the contact angle, γ_{SV}, γ_{SL}, and γ_{LV} are the surface tensions of solid−vapor, solid−liquid, and liquid−vapor, respectively. For $\phi = 0°$, the liquid droplet spreads over entire solid surface. At $\phi < 90°$, the liquid droplet wets the solid. The liquid does not wet solid for $\phi > 90°$, especially when $\phi = 180°$. The contact angle can be determined using sessile drop measurements. In general, ceramic nanoparticle has poor wettability with molten metal. This issue can be addressed partly by mixing ceramic nanoparticles with reactive metals, such as Mg and Li, using ball milling or heat treatment [17,18].

Alternatively, better dispersion of reinforcing particles can be realized by reducing the casting temperature via compocasting or rheocasting process, in which the reinforcements are added to metal in a semisolid state. For conventional MMCs, compocasting enables the attainment of improved wettability and better distribution of ceramic microparticles compared to stir casting [19,20]. Accordingly, this process has been employed increasingly by the researchers to fabricate cast MMNCs [16,21]. In some cases, compocasting-assisted ultrasonic cavitation can achieve even more uniform dispersion of ceramic nanoparticles [13−16]. The ultrasonic probe system can generate intense transient cavitation at a temperature of ∼5000°C and pressure of ∼1000 atm. The probe induces a violent collapse of micro gas bubbles around nanoparticle clusters, thereby causing breakdown of the clusters in the melt.

8.2.1.1 *Al-Based Nanocomposites*

Tahamtan et al. [18] employed mechanical stir mixing to fabricate 5 vol% Al_2O_3p/A206 nanocomposite. The A206 alloy consists of 4.2−5.0% Cu, 0.2−0.5% Mg, 0.15−0.35% Mn, 0.15−0.3% Ti, <0.05% and Al balance. Below 1000°C, the contact angle between aluminum and Al_2O_3 is >90°, resulting in poor wetting by the liquid metal. This poor wetting behavior favors clustering of the alumina particles and their floating on the surface of the melt. To improve wettability of alumina nanoparticles (100 nm), alumina nanoparticles were ball-milled with Mg and Al powders followed by compression into disc specimens. Ball-milled discs were introduced into molten A206 alloy for forming nanocomposite. As a result, wettability of ball-milled alumina with molten metal improves considerably, leading to

better distribution of nanoparticles in the melt. Mazahery et al. [22] also ball milled alumina nanoparticles (50 nm) with Al particles (16 μm) prior to introduction to molten A356 aluminum alloy. A356 is a hypoeutectic Al−Si alloy with a nominal composition of 7.5 wt% Si, 0.38 wt% Mg, 0.02 wt% Zn, 0.107 wt% Fe, and Al balance.

Very recently, Sajjadi et al. [19] fabricated Al_2O_3/A356 nanocomposites using both stir casting and compocasting processes. They reported that the alumina nanoparticles act as effective nucleation sites for the Al grains, producing nanocomposites with fine-grained microstructure. Due to the improved wettability of particles with the melt during compocasting, the grain size of compocast nanocomposite is finer than that of stir-cast composite (Figure 8.4A−C). Moreover, compocast nanocomposites have lower porosity content than stir-cast materials. Similarly, El-Mahallawi et al. [23] also reported that compocast Al_2O_3/A356 nanocomposites show good distribution and low agglomeration of alumina nanoparticles in the alloy matrix.

Li et al. [13] fabricated SiC/A356 nanocomposite by means of ultrasonic vibration processing for enhancing dispersion of ceramic nanoparticles. Figure 8.5 is a schematic diagram showing the setup of a typical ultrasonic processing system. The optical images of the A356 alloy and its nanocomposite with 2 wt% SiC are

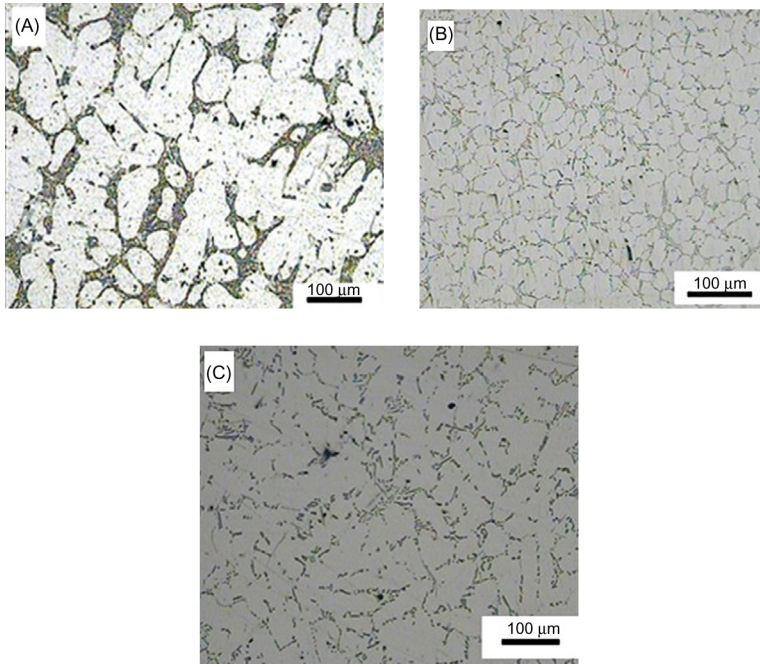

Figure 8.4 Optical images of (A) cast A356 alloy, (B) compocast 1 wt% Al_2O_3/A356 nanocomposite, and (C) stir-cast 1 wt% Al_2O_3/A356 nanocomposite.
Source: Reprinted from Ref. [19] with permission of Elsevier.

shown in Figure 8.6A–C, respectively. The microstructure reveals the formation of aluminum dendrites surrounded by a network of eutectic Al–Si lamellae. In a recent study, they also introduced 1.5 vol% TiCN nanoparticles into molten Al–9Mg alloy under ultrasonic mixing at 715°C [15]. The resulting composite showed significant grain refinement with TiCN nanoparticles dispersed mainly at the grain boundaries of matrix alloy (Figure 8.7A and B).

Su et al. [16] fabricated Al_2O_3/AA2024 nanocomposites using compocasting-assisted ultrasonic vibration. Figure 8.8A shows the microstructure of cast 1 wt% Al_2O_3/AA2024 nanocomposite. The nanocomposite exhibits fine-grained morphology. Alumina nanoparticles are well dispersed within the grains and at the grain boundaries of the matrix alloy (Figure 8.8B and C). The microstructural evolution of the composite melt during the solidification under an ultrasonic field is shown in Figure 8.9. During the solidification, primary α-Al dendrites first nucleate in the

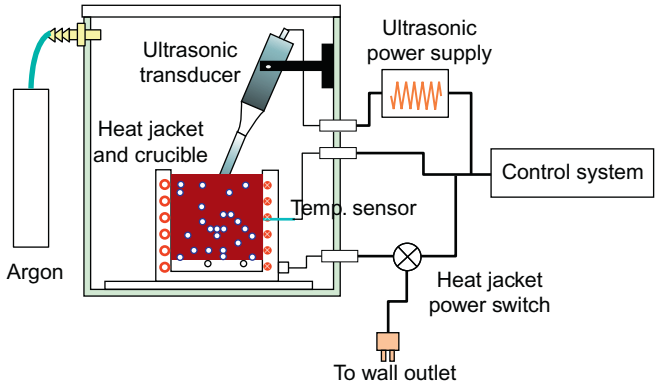

Figure 8.5 Experimental setup for ultrasonic processing unit.
Source: Reprinted from Ref. [13] with permission of Elsevier.

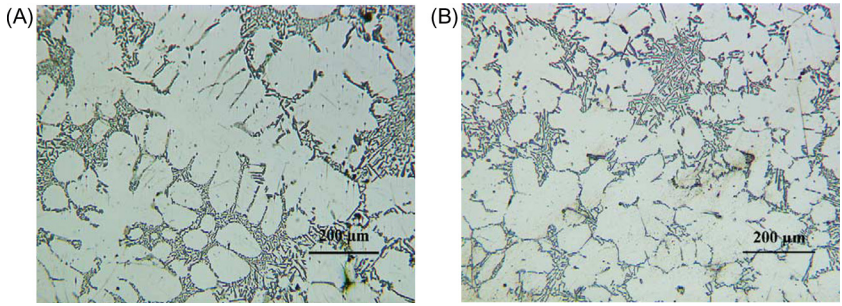

Figure 8.6 Microstructures of as-cast (A) A356 alloy without ultrasonic treatment and (B) 2 wt% SiC/A356 nanocomposite with ultrasonic processing.
Source: Reprinted from Ref. [12] with permission of Elsevier.

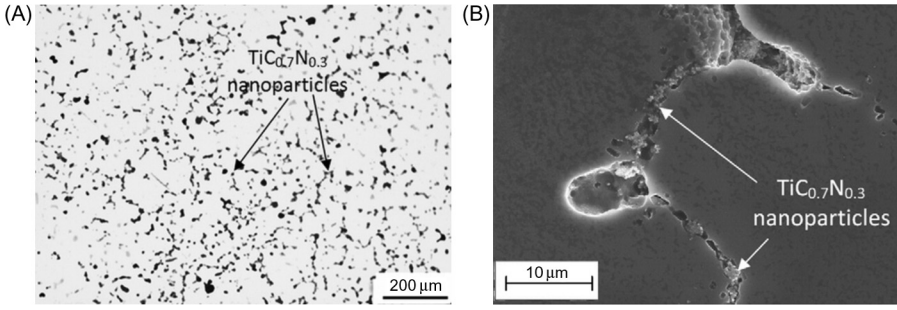

Figure 8.7 (A) Optical micrograph of unetched 1.5 vol% TiCN/Al−9Mg composite. (B) SEM micrograph of etched 1.5 vol% TiCN/Al−9Mg composite showing nanoparticles distributed along the grain boundaries.
Source: Reprinted from Ref. [15] with permission of Elsevier.

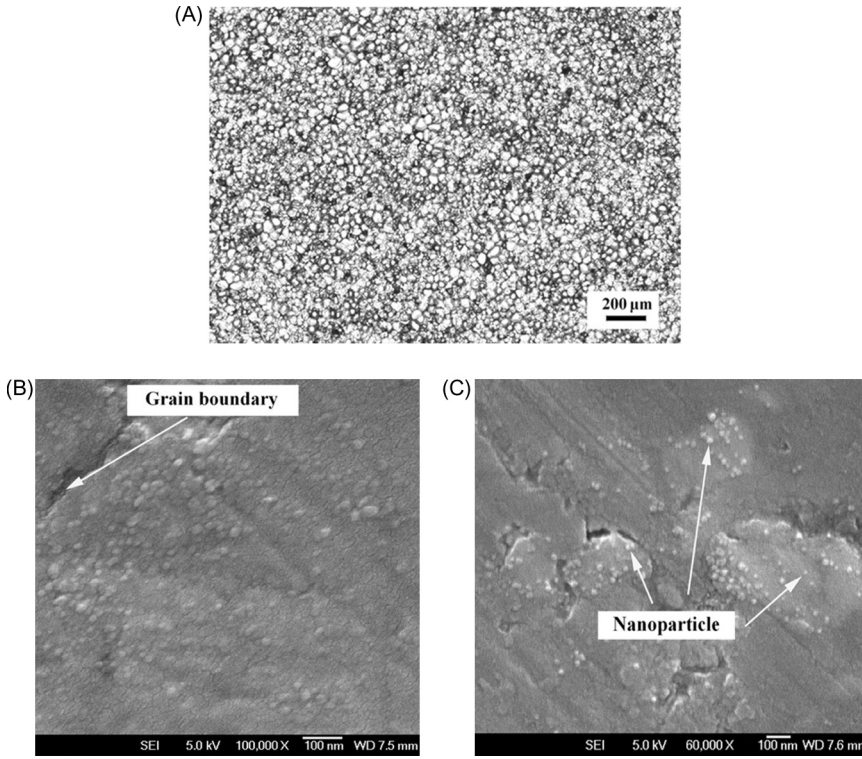

Figure 8.8 Microstructure of Al_2O_3/AA2024 nanocomposite prepared under ultrasonic vibration. (A) Optical micrograph. SEM images showing (B) grain interior and (C) grain boundary.
Source: Reprinted from Ref. [16] with permission of Elsevier.

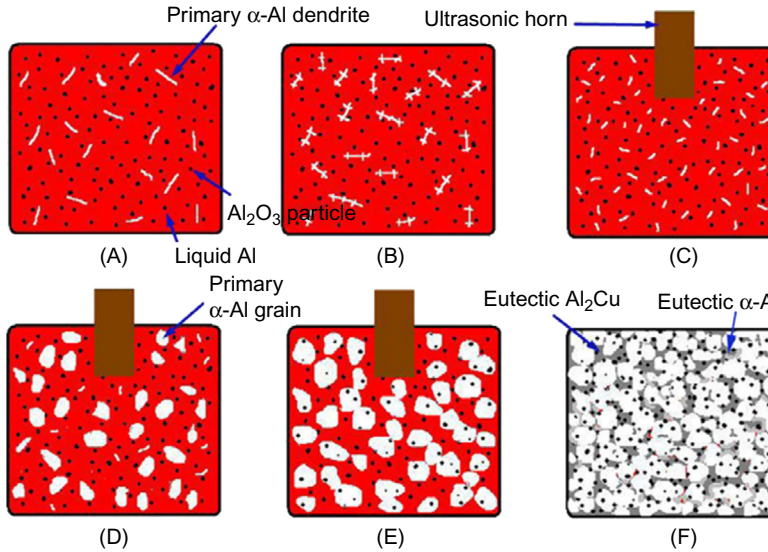

Figure 8.9 Scheme of evolution of Al_2O_3/AA2024 nanocomposite melt to final microstructure under an ultrasonic field: (A) the formation of primary α-Al dendrites, (B) the formation of dendritic arms, (C) the breakage of dendrites by ultrasonic cavitation, (D and E) the growth of α-Al grains, and (F) the completion of the solidification. *Source*: Reprinted from Ref. [16] with permission of Elsevier.

melt, while alumina nanoparticles are pushed into the melt by the dendrites (Figure 8.9A and B). When an ultrasonic probe is introduced into the melt, the dendrites are broken by intense ultrasonic cavitation, producing more nucleation sites for the α-Al grains (Figure 8.9C and D). Some alumina nanoparticles are trapped inside the grains under intensive ultrasonic cavitation (Figure 8.9E). As the temperature of the composite slurry drops to the solidus temperature, the eutectic reaction takes place eventually. Those alumina nanoparticles pushed by the growing grains are trapped within the eutectic phase (Figure 8.9F).

8.2.1.2 Mg-Based Nanocomposites

Magnesium has a density of 1.74 g/cm^3, that is, about two-thirds of the density of aluminum with a value of 2.70 g/cm^3. Magnesium offers several advantages for structural engineering applications, including good damping capacity, excellent castability, and large abundance. Comparing with Al, magnesium possesses low mechanical strength, poor creep, and corrosion resistance. Magnesium alloys with hexagonal close-packed (HCP) lattice are difficult to deform mechanically at room temperature due to their limited numbers of slip system. Despite these shortcomings, light-weight magnesium alloys have attracted increasing attention for use as structural materials in the automotive and aerospace industries recently because of

the weight-reduction consideration [24]. Typical examples are the AZ series having Al contents ≤ 9 wt%, including AZ31 (Mg−3Al−1Zn−0.2Mn) and AZ91 (Mg−9Al−1Zn−0.3Mn) alloys. Zinc is added to improve the corrosion resistance and strength of magnesium alloys. Generally, the low mechanical strength of Mg-based alloys can be improved greatly by adding ceramic nanoparticles.

Li and coworkers fabricated Mg-based MMCs reinforced with SiC or AlN nanoparticles using ultrasonic cavitation method [13,14,25,26]. The additions of SiC nanoparticles to Mg under ultrasonic-assisted casting process result in a significant reduction of the matrix grain size. However, some SiC microclusters still exist in the microstructures, especially at the grain boundaries [25,26]. High-resolution TEM image shows a clean interface between the Mg matrix and SiC nanoparticles (Figure 8.10A and B). In another study, the dispersion of AlN nanoparticles in the alloy matrix is somewhat improved. Figure 8.11A and B shows low magnified SEM images of cast AZ91D alloy and 1 wt% AlN/AZ91D nanocomposite, respectively. The microstructure of AZ91D is mainly composed of α-Mg, massive β-phase and lamellar β-$Mg_{17}Al_{12}$ phase. The microstructure of 1 wt% AlN/AZ91D nanocomposite is similar to that of AZ91D, but with much finer β-phase, demonstrating that a small loading level of AlN nanoparticles affects the solidification process of AZ91D alloy. At high magnification image, AlN nanoparticles tend to disperse into individual particles in the alloy matrix (Figure 8.11C). Very recently, Nie et al. [27,28] employed ultrasonic vibration during stir casting or compocasting to fabricate 1 vol% SiC/AZ91 nanocomposite. In the latter process, AZ91 alloy was first heated to 700°C, followed by cooling to 590°C in which the alloy was in a semisolid state. 1 vol% SiC nanoparticles (60 nm) were quickly added into the semisolid alloy under mechanical stirring for 5, 10, or 15 min. The melt was then reheated to 700°C and an ultrasonic probe was dipped into the melt for dispersing SiC nanoparticles (Figure 8.12).

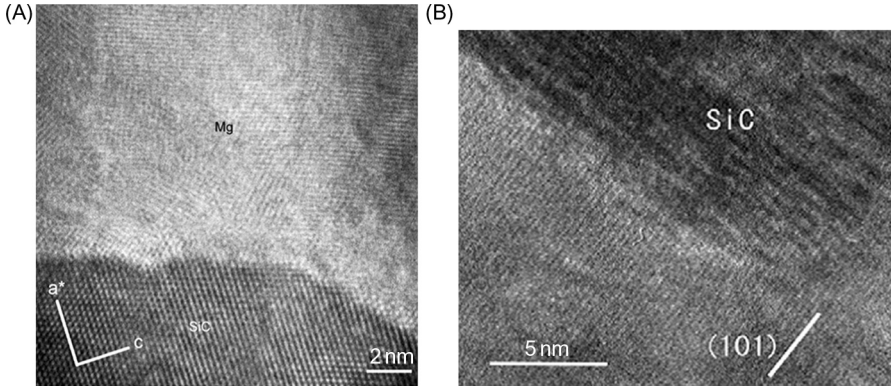

Figure 8.10 High-resolution TEM images showing a clean Mg−SiC interface in (A) 1 wt% SiC/Mg and (B) 2 wt% SiC/Mg−4Al−1Si nanocomposites.
Source: Reprinted from Refs. [25,26] with permission of Elsevier.

Gupta and coworkers systematically studied the microstructure and mechanical behavior of magnesium-based composites reinforced with alumina nanoparticles prepared by disintegrated melt deposition (DMD) technique [29–33]. The process involves mechanical stirring of Mg chips and reinforcing particles using an

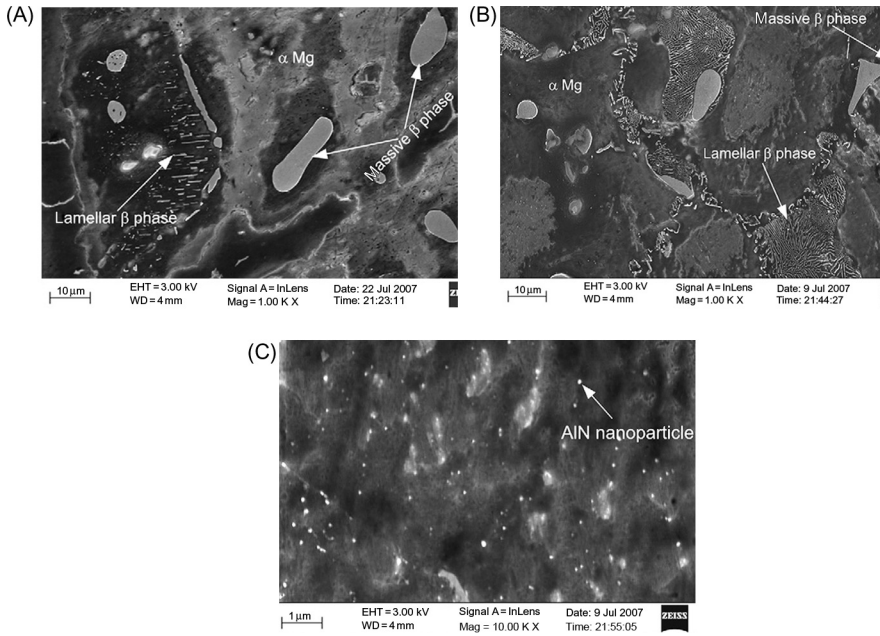

Figure 8.11 Low magnified SEM images of (A) AZ91D alloy and (B) 1 wt% AlN/AZ91D nanocomposite. (C) High magnification SEM image of 1 wt% AlN/AZ91D nanocomposite. *Source*: Reprinted from Ref. [14] with permission of Elsevier.

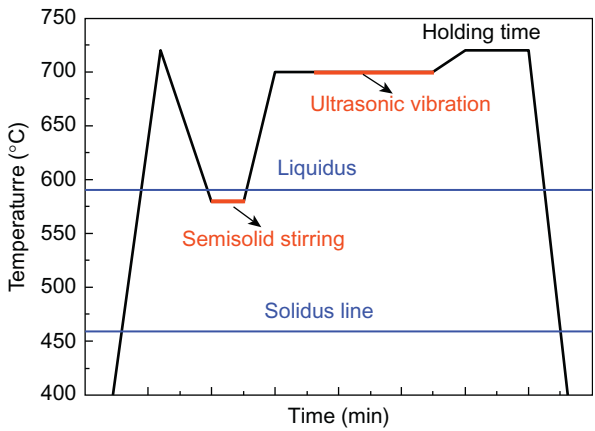

Figure 8.12 Schematic illustration of the temperature–time sequences for semisolid stirring assisted ultrasonic vibration. *Source*: Reprinted from Ref. [28] with permission of Elsevier.

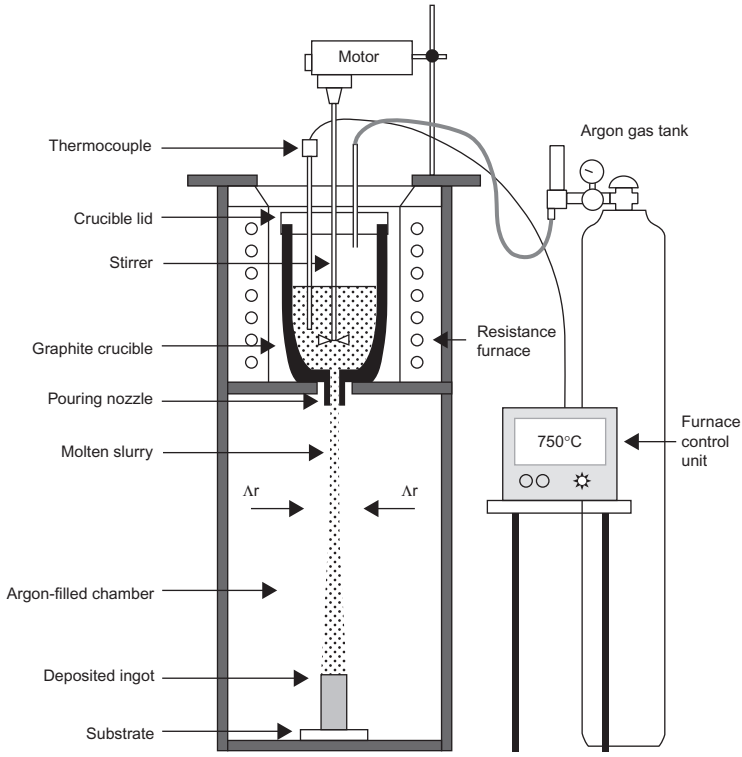

Figure 8.13 Schematic representation of DMD process.
Source: Reprinted from Ref. [34] with permission of Elsevier.

impeller under an argon atmosphere at a superheat temperature of 750°C (Figure 8.13) [34]. The melt was released through a pouring nozzle located at the base of crucible and disintegrated with argon gas jets. The ingot was hot extruded eventually. Microstructural examinations of the extruded composite samples revealed fairly uniform distribution of alumina nanoparticles.

8.2.2 Solid-State Processing

PM technique is a versatile process for manufacturing MMNCs due to its simplicity, flexibility, and near net-shape capability. The process involves mechanical blending of ceramic nanoparticles with metal/alloy powders in a rotary mill, followed by cold compaction and sintering. By simply mixing metal powders with the reinforcement material, homogeneous dispersion of nanoparticles in the metal matrix is difficult to achieve, especially at higher particle contents. The dispersion of ceramic nanoparticles can be somewhat improved through a wet mixing method in which the composite constituents are suspended in a solvent (e.g., ethanol),

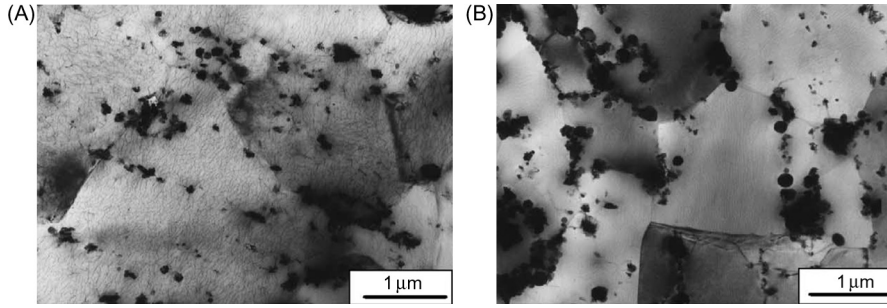

Figure 8.14 TEM micrographs of (A) 1 vol% Al_2O_3/Al and (B) 4 vol% Al_2O_3/Al nanocomposites.
Source: Reprinted from Ref. [35] with permission of Elsevier.

followed by the solvent evaporation, cold compaction, and sintering [35]. Figure 8.14A and B shows TEM micrographs of 1 vol% Al_2O_3/Al and 4 vol% Al_2O_3/Al nanocomposites prepared by wet powder mixing and sintering. Alumina nanoparticles together with few clusters are dispersed fairly in the Al matrix of 1 vol% Al_2O_3/Al nanocomposite. By increasing the particle content to 4 vol%, alumina nanoparticle clusters within the grains and at the matrix grain boundaries can be readily seen in the micrograph.

Mechanical alloying (MA) process is known to be effective for dispersing ceramic nanoparticles homogeneously in the metal matrix [36]. A uniform distribution of ceramic nanoparticles in the metal matrix is the crucial factor for attaining enhanced mechanical properties of MMNCs. MA is a solid-state processing that involves loading constituent powders into a high-energy ball mill containing grinding media, such as stainless steel or alumina balls. The powder mixture undergoes a series of repeating fracture, deform, and welding processes. This leads to intimate mixing of constituent powder particles on an atomic scale, producing a variety of supersaturated solid solutions, metastable crystallites, amorphous metal alloys, and grain size refinement down to nanometer scale. This process is commonly used to produce alloys and composites that are difficult to obtain from conventional melting and casting techniques. A process control agent (PCA), such as stearic acid or acrylic acid, is occasionally added. The PCA adsorbs on the surface of powder particles and minimizes cold welding between impacted particles, thereby preventing agglomeration. To minimize oxidation during high-energy milling, the operation can be carried out at cryogenic temperatures by introducing liquid nitrogen into the milling chamber. This process is termed as cryomilling. Several factors, such as the charge ratio (ratio of the weight of balls to the powder), ball mill design, milling atmosphere, time, speed, and temperature, can affect the dispersion of nanoparticles in metallic powders.

In recent years, FSP becomes quite popular for fabricating surface composites with ultrafine-grained microstructures via dynamic recrystallization [37]. In the process, a rotating tool pin is inserted to the substrate such that the friction and

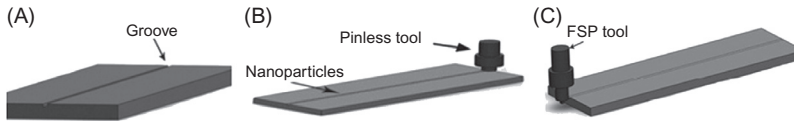

Figure 8.15 Schematic of the FSP process: (A) cutting a groove on the plate, (B) filling the groove with ceramic nanopowder and covering it with a pinless tool, and (C) performing FSP process with a pin tool.
Source: Reprinted from Ref. [38] with permission of Elsevier.

plastic deformation induced by the tool heats and softens the work piece. The tool pin then promotes intermixing of material in a local region. To manufacture MMNCs, a long groove cut on a metal surface in the path of the tool is filled with ceramic nanoparticles Then, the FSP is conducted along the groove to produce a thick surface composite (Figure 8.15) [38]. FSP can also serve as a secondary mechanical processing tool for achieving homogeneous dispersion of reinforcing nanoparticles and eliminating internal defects in the cast MMNCs [38,39].

8.2.2.1 Al-Based Nanocomposites

Razavi Hesabi et al. [40] studied morphological evolution and structural change of the Al_2O_3/Al composites by milling 5 vol% nano-Al_2O_3 (35 nm) and micro-Al_2O_3 (1 μm) to pure Al (48 μm) in a planetary ball mill under an argon atmosphere. They reported that the milling stages, such as plastic deformation, microwelding, and particle fragmentation, occur earlier in the composite with microalumina particles than in the powder mixture with nanoalumina particles. Furthermore, longer milling time is needed to achieve the steady-state condition in nanoalumina-reinforced composite. Zebarjad and Sajjadi [41,42] indicated that alumina micropowders became finer and dispersed more uniformly in aluminum with increasing milling time.

Bathula et al. [43] employed high-energy ball milling and SPS to fabricate SiC/AA5083 composite. AA5083 alloy (Al−4.5Mg, 0.9Mn, 0.4Si, 0.2Cu, 0.15Ti, 0.25Zn) powder with a size of ∼15 μm was ball milled with 10 wt% SiC nanoparticles (∼20 nm) for 15 h. Figure 8.16A and B is SEM images of the as-received AA5083 alloy and milled SiC/AA5083 composite for 15 h. The milled composite mixture exhibits faceted feature with sizes ranging from 40 to 50 μm. A large increase in the size of milled composite mixture is due to the powder constituents undergoing a series of welding and fracture of particles process during the MA process. By consolidating with SPS, a dense nanocomposite with homogeneous dispersion of SiC nanoparticles in the metal matrix is obtained (Figure 8.17A and B). Kollo et al. [44] employed both planetary and attritor ball milling with heptane as a milling agent to fabricate SiC/Al nanocomposites. In spite of different milling techniques employed, effective dispersion of SiC nanoparticles in the aluminum matrix was achieved.

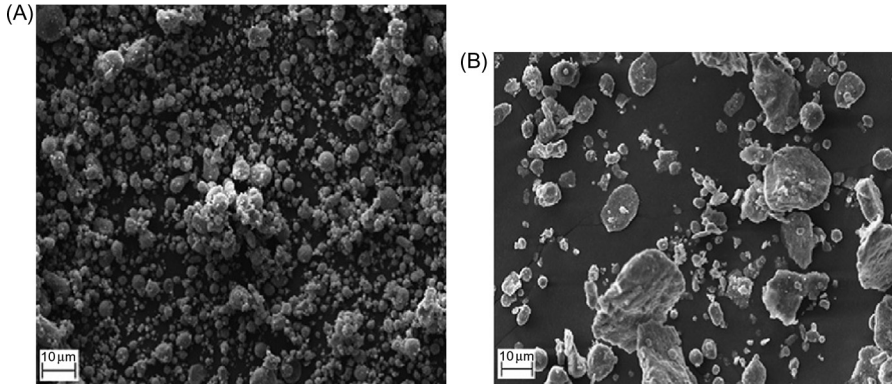

Figure 8.16 SEM images of (A) as-received AA5083 alloy and (B) SiC/AA5083 composite mixture after high-energy ball milling for 15 h.
Source: Reprinted from Ref. [43] with permission of Elsevier.

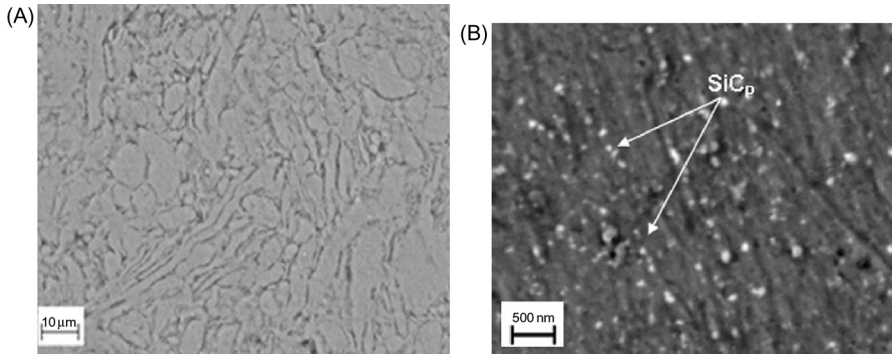

Figure 8.17 SEM images of spark plasma sintered SiC/AA5083 nanocomposite showing (A) dense feature and (B) dispersion of SiC nanoparticles.
Source: Reprinted from Ref. [43] with permission of Elsevier.

Recently, Shafiei-Zarghani et al. [45] employed FSP to fabricate Al_2O_3/Al composites. Their results showed alumina nanoparticles can disperse more uniformly in the metal matrix by increasing the number of FSP passes. Sharifitabar et al. [46] also reported a similar finding. They investigated the effects of processing parameters on microstructural evolution, deformation, and mechanical behavior of the nanocomposites. Bauri et al. [39] used FSP to homogenize the particle distribution in the cast 5 wt% TiC/Al composite. A single pass of FSP was enough to break the particle clusters. Two passes of FSP resulted in complete homogenization and elimination of casting defects. The grain size of the metal matrix was also refined substantially after each FSP pass.

8.2.2.2 Mg-Based Nanocomposites

Hassan and Gupta fabricated 1.1 vol% Al_2O_3/Mg nanocomposite by means of simple powder mixing and sintering [30]. Wong and Gupta also prepared SiC/Mg nanocomposites using dry powder mixing and microwave sintering [47]. Microwave sintering allows rapid densification of green products for short periods of time at lower temperatures. Ferkel and Mordike employed simple powder mixing or ball milling SiC nanoparticles (30 nm) with Mg powder (40 μm) followed by hot extrusion to fabricate 3 vol% SiC/Mg nanocomposite specimens [48]. For extruded composite prepared by powder mixing, SiC nanoparticles dispersed at the grain boundaries of coarse and elongated magnesium grains. For extruded composite fabricated by ball milling, SiC nanoparticles dispersed mainly at the shear bands of heavily deformed magnesium grains, with some nanoparticles located at fined magnesium grains of submicrometer scale.

FSP is an effective tool to eliminate casting defects of magnesium alloys. As aforementioned, the microstructure of cast AZ91 alloy consists of irregularly distributed β-$Mg_{17}Al_{12}$ phase at its grain boundaries (Figure 8.11A). The microstructure of FSPed AZ91-based nanocomposites is characterized by the homogeneous distribution of ceramic nanoparticles, the recrystallized grain structure, and the dissolution of β phase [38,49].

8.3 Mechanical Properties

The addition of second-phase particles in a crystal matrix is a common method for improving the mechanical properties of materials. In general, the additions of ceramic nanoparticles to metals increase the Young's modulus, yield stress, and tensile strength of MMNCs. The strengthening mechanisms responsible for the yield strength enhancement, include Orowan strengthening, grain size refinement due to the Hall−Petch effect, creation of dislocations to accommodate thermal expansion mismatch between the reinforcement and the matrix, and the load-bearing effect of the reinforcement. Among them, Orowan strengthening plays a decisive role in enhancing the yield strength of MMNCs due to the nanoscale dimension of reinforcing particles. These nanoparticles impede the movement of dislocations through dislocation bowing and looping effects. The bowing of dislocations between the nanoparticles builds up dislocation loops around each nanoparticle. On the other hand, Orowan strengthening is insignificant in the MMCs reinforced with microparticles, because the reinforcing particles are coarse and thus the interparticle spacing is large. The increment in yield stress due to Orowan strengthening can be described by the Orowan−Ashby equation [50]:

$$\Delta\sigma = \frac{0.13Gb}{\lambda}\ln\frac{r}{b} \tag{8.3}$$

where G is the shear modulus of the matrix material, b the burgers vector, r the radius of the particle, and λ the interparticle spacing defined by

$$\lambda = d_p\left[\left(\frac{1}{2V_p}\right)^{1/3} - 1\right] \tag{8.4}$$

where V_p and d_p are the volume fraction and diameter of the nanoparticle, respectively. By decreasing the size of reinforcements to nanoscale level, the interparticle spacing is reduced, thereby restricting the activities of dislocations more effectively. The Orowan effect becomes less significant for the MMNCs with ceramic nanoparticles mainly located at the matrix grain boundaries.

The incorporation of ceramic nanoparticles into metals/alloys can lead to grain refining of the matrix phase. The yield strength enhancement of a composite due to the matrix grain refining can be described by the Hall−Petch equation:

$$\Delta\sigma_{HP} = \sigma_o + kd^{-1/2} \tag{8.5}$$

where d is the grain size, σ_o is friction stress, which includes contributions from the solutes and particles, and k is the Hall−Petch slope, that is, a measure of the resistance to dislocation motion caused by the presence of grain boundaries. The yield strength contribution by the dislocations generated from the difference in coefficient of thermal expansion between the reinforcement phase and the matrix can be written as [51]

$$\Delta\sigma_{CTE} = \sqrt{3}\alpha Gb\sqrt{\rho} \tag{8.6}$$

where ρ is the dislocation density and α the strengthening coefficient. This stress depends on the temperature from which the composite is cooled from its fabrication temperature. The load-bearing effect generally is insignificant in MMNCs with ceramic nanoparticles of a small aspect ratio, i.e., unity. The shear transfer of load from the soft matrix to the hard ceramic reinforcements during mechanical deformation can be expressed as [52]

$$\Delta\sigma_{load} = 0.5V_p\sigma_{ym} \tag{8.7}$$

where σ_{ym} is the matrix yield stress.

From these, the final yield strength of an MMNC is a linear summation of the strength imparted by each mechanism. Considering Orowan strengthening, dislocation generation, and load-bearing effects, Zhang and Chen derived the following equations for the yield stress of a composite (σ_{yc}) [52]:

$$\sigma_{yc} = (1 + 0.5V_p)\left(\sigma_{ym} + A + B\frac{AB}{\sigma_{ym}}\right) \tag{8.8}$$

$$A = 1.25 G_m b \sqrt{\frac{12(T_{process} - T_{test})(\alpha_m - \alpha_p)V_p}{b d_p (1 - V_p)}} \tag{8.9}$$

$$B = \frac{0.13 G_m b}{d_p \left[(1/2V_p)^{1/3} - 1\right]} \ln \frac{d_p}{2b} \tag{8.10}$$

where G_m is the shear modulus of the matrix, $T_{process}$ is the processing temperature, T_{test} is the testing temperature, α_m and α_p are the coefficient of thermal expansion of the matrix and particle, respectively.

8.3.1 Al-Based Nanocomposites

8.3.1.1 Nanocomposites Fabricated by Liquid-State Processing

The mechanical performance of MMNCs depends greatly on the attainment of homogeneous dispersion of ceramic nanoparticles in the metal matrix. Agglomeration of ceramic nanoparticles often occurs in the composites fabricated by liquid metallurgy route owing to the poor wettability of nanoparticles by molten metal. In this regard, special measures have been taken in the melt practices for enhancing wettability of ceramic nanoparticles. Mazahery et al. [22] fabricated Al_2O_3/A356 nanocomposites by stir casting at 800°C. Prior to the composite fabrication, alumina nanoparticles were ball-milled with Al particles to improve their wettability with liquid metal. Porosity level in the nanocomposites increased slightly with increasing particulate volume content due to the increase of contact surface area of alumina nanoparticles with molten aluminum alloy. Table 8.1 summarizes tensile behavior of stir-cast Al_2O_3/A356 nanocomposites. The yield strength, tensile strength, and ductility of the nanocomposites improved with the increase in alumina content. Furthermore, the tensile strength of 1.5 vol% Al_2O_3/A356 nanocomposite using Al particles is much higher than that of 1.5 vol%

Table 8.1 Tensile Properties of Stir-Cast Al_2O_3/A356 Nanocomposites

Materials	Casting at	Tensile Strength (MPa)	Ductility (%)	Grain Size (μm)
Al	800°C	115 ± 3	2.9	48
1.5 Al_2O_3/Al without using Al particles	800°C	126 ± 4	1.4	45
0.75 Al_2O_3/Al using Al particles	800°C	167 ± 2	2	16
1.5 Al_2O_3/Al using Al particles	800°C	182 ± 2	2.2	12
2.5 Al_2O_3/Al using Al particles	800°C	171 ± 2	2	15
3.5 Al_2O_3/Al using Al particles	800°C	163 ± 2	1.9	14
5 Al_2O_3/Al using Al particles	800°C	160 ± 3	1.7	15

Source: Reprinted from Ref. [22] with permission of Elsevier.

Al_2O_3/A356 nanocomposite without milling alumina with Al particles. More recently, Karbalaei Akbari et al. [53] also ball milled alumina nanoparticles with either Al or Cu powders. They fabricated 1.5 vol% Al_2O_3/A356 nanocomposite by casting at 850°C under mechanical stirring at different periods. They found that the porosity level increased with increasing stirring time. Thus, the yield stress and Young's modulus of the nanocomposite decrease with increasing stirring time (Figure 8.18A and B). It is noted that the as-cast A356 alloy exhibits low tensile ductility (only 0.7%). The stir-cast nanocomposite also exhibits low tensile ductility due to the formation of dendritic structure and porosity (Figure 8.19).

Sajjadi et al. [19] compared the microstructure and mechanical behavior of stir-cast and compocast Al_2O_3/A356 nanocomposites. They also fabricated Al_2O_3/A356 microcomposites using the same casting processes for the purposes of comparison. The mechanical results showed that the addition of alumina (micro and nano) to A356 led to the improvement in yield strength, ultimate tensile strength, compression strength, and hardness at the expense tensile ductility. They attributed this to the matrix grain size refinement and the creation of thermal mismatch dislocations due to the additions of reinforcing particles. Moreover, compocast nanocomposites exhibit higher yield stress and tensile strength than stir-cast nanocomposites. The porosity level and grain size of compocast nanocomposites were lower than those of stir-cast materials because the wettability of particles in compocasting was better than stir casting. Figure 8.20 shows typical stress−strain curves of A356 and its nanocomposites fabricated by compocasting. The variations of yield stress and

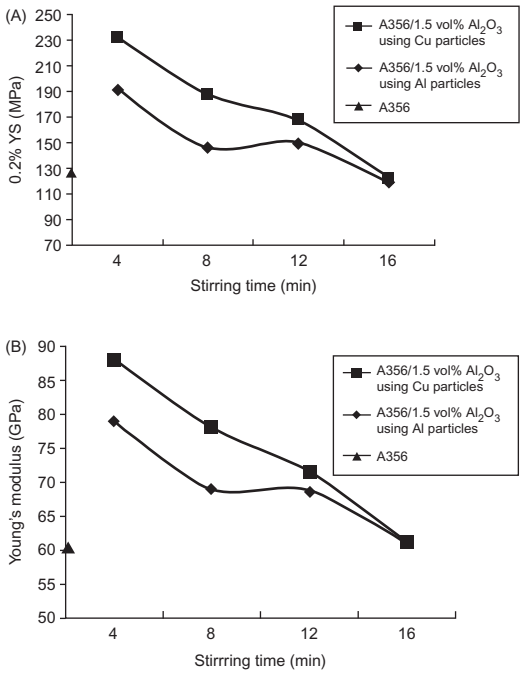

Figure 8.18 The variations of (A) yield strength and (B) Young's modulus with stirring time for stir-cast 1.5 vol% Al_2O_3/A356 nanocomposite materials.
Source: Reprinted from Ref. [53] with permission of Elsevier.

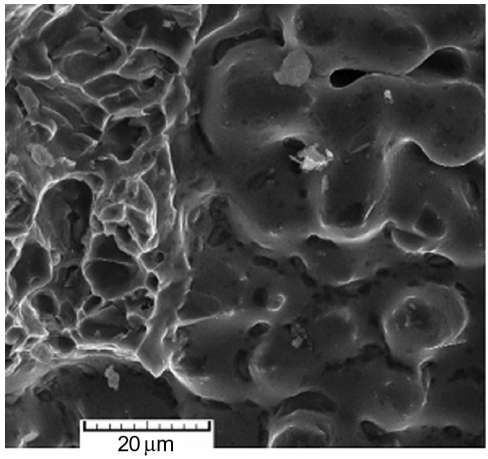

Figure 8.19 SEM fractograph of tensile-tested 1.5 vol% Al_2O_3/A356 nanocomposite showing dendritic feature and porosity.
Source: Reprinted from Ref. [53] with permission of Elsevier.

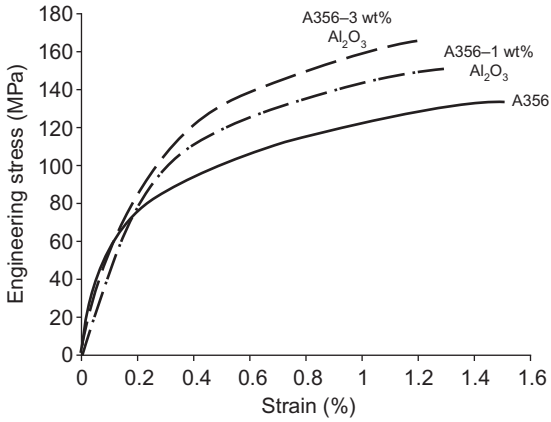

Figure 8.20 Tensile stress−strain curves of A356 and its nanocomposites fabricated by compocasting.
Source: Reprinted from Ref. [19] with permission of Elsevier.

ultimate tensile strength with alumina content of both micro- and nanocomposites are shown in Figure 8.21A and B, respectively.

Li and coworkers fabricated Al-based nanocomposites reinforced with SiC or TiCN nanoparticles using ultrasonic cavitation processing method [12,15]. Figure 8.22A shows the variations of yield stress and tensile strength with SiC nanoparticle content of SiC/A356 nanocomposites. The elongation versus nanoparticle content of the SiC/A356 nanocomposites is shown in Figure 8.22B. Apparently, SiC nanoparticle additions enhance the yield stress of A356 alloy markedly without sacrificing tensile ductility. The yield stress of A356 alloy is improved more than 50% by adding 2 wt% SiC nanoparticles. Su et al. [16] fabricated Al_2O_3/AA2024 nanocomposites using compocasting-assisted ultrasonic cavitation. Figure 8.23 shows tensile properties of as-cast AA2024 and its nanocomposites. Optimal yield stress and tensile strength of AA2024 can be achieved by adding 1 wt% alumina nanoparticles. Comparing with the matrix alloy,

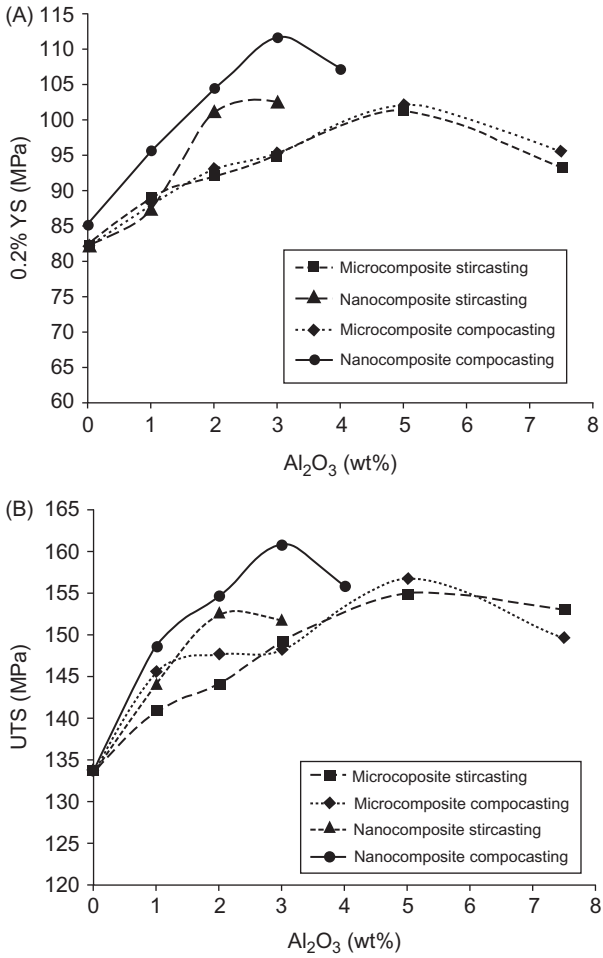

Figure 8.21 The variations of (A) 0.2% yield strength and (B) ultimate strength with alumina content of compocast and stir-cast composites. *Source*: Reprinted from Ref. [19] with permission of Elsevier.

the ultimate tensile strength and yield strength of 1 wt% Al_2O_3/AA2024 composite are enhanced by 37 and 81%, respectively. This is attributed to homogeneous distribution of alumina nanoparticles and grain refinement of the aluminum matrix (Figure 8.8). Representative tensile properties of cast MMNCs reported by several researchers are summarized in Table 8.2. In this table, the content of ceramic nanoparticles is given in volume percentage or weight percentage. The relation between the volume fraction (V_f) and weight fraction (W_f) of the reinforcing phase of a composite is given by

$$V_f = \frac{W_f/\rho_f}{(W_f/\rho_f) + (1 - W_f)/\rho_m} = \frac{W_f \rho_m}{W_f \rho_m + (1 - W_f)\rho_f} \tag{8.11}$$

where ρ_f and ρ_m are the reinforcing phase density and matrix density.

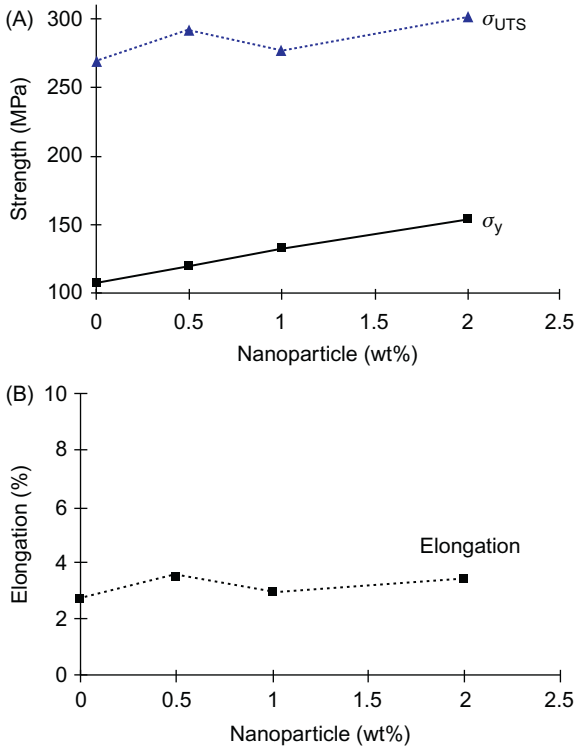

Figure 8.22 (A) Yield stress and tensile strength and (B) elongation versus SiC nanoparticle content of SiC/A356 nanocomposites. *Source*: Reprinted from Ref. [12] with permission of Elsevier.

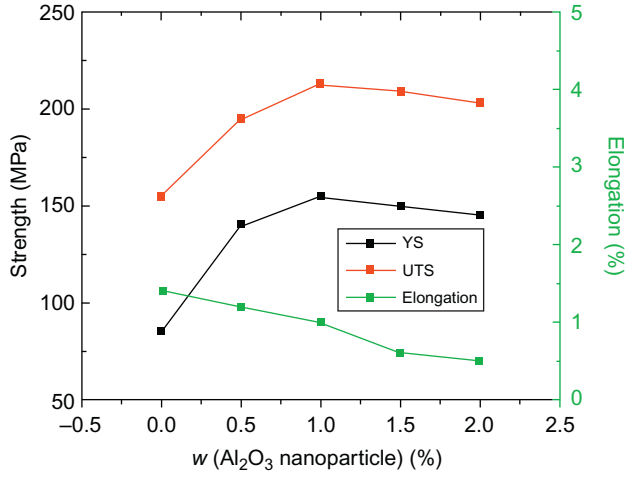

Figure 8.23 Tensile properties of as-cast AA2024 and Al_2O_3/AA2024 nanocomposites. *Source*: Reprinted from Ref. [16] with permission of Elsevier.

Table 8.2 Tensile Properties of Cast Aluminum Matrix Nanocomposites

Particle Content (vol%)	Particle Content (wt%)	Reinforcing Nanoparticle	Matrix Material	Fabrication Process	Yield Strength (MPa)	Tensile Strength (MPa)	Fracture Strain (%)	References
0	–	–	A356	Stir casting	94	135	–	[22]
1.5	–	Al_2O_3	A356	Stir casting at 800°C for 15 min	115	182	2.2	[22]
0	–	–	A356	Stir casting	127	137	0.7	[53]
1.5	–	Al_2O_3	A356	Stir casting at 850°C for 4 min	190	213	0.91	[53]
1.5	–	Al_2O_3	A356	Stir casting at 850°C for 12 min	150	168	0.58	[53]
	0	–	A356	Stir casting	85	134	1.55	[19]
	1	Al_2O_3	A356	Stir casting at 700°C for 30 min	88	143	1.31	[19]
	1	Al_2O_3	A356	Compocasting at 610°C	104	148	1.37	[19]
	3	Al_2O_3	A356	Stir casting at 700°C for 30 min	102	152	1.12	[19]
	3	Al_2O_3	A356	Compocasting at 610°C	112	160	1.19	[19]
0	–	–	Al–9Mg	Melting at 715°C assisted with ultrasonic vibration	137	167	1.4	[15]
0.5	–	TiCN	Al–9Mg	1.5 vol% TiCN/Al–9Mg nanocomposite was added to Al–9Mg melt for dilution	143	200	2.7	[15]
1.5	–	TiCN	Al–9Mg	Melting at 715°C assisted with ultrasonic vibration	146	209	2.9	[15]

8.3.1.2 Nanocomposites Fabricated by Solid-State Processing

Tjong et al. [10] were the first researchers to report the tensile behavior of aluminum reinforced with 1 vol% Si_3N_4 nanoparticles (15 nm). The nanocomposite was fabricated by dry powder mixing followed by hot pressing and hot extrusion. The results showed that the Si_3N_4 nanoparticles are very effective to enhance the yield stress and tensile strength of Al. The yield stress of Al increases significantly from 68 to 144 MPa by adding 1 vol% Si_3N_4. They attributed this to the Orowan strengthening mechanism. Kang and Chan [35] then also reported that low volume fractions of alumina nanoparticles are beneficial in improving yield stress and tensile strength of aluminum (Figure 8.24). The tensile strength of 1 vol% Al_2O_3/Al nanocomposite is similar to that of the 10 vol% SiCp (13 μm)/Al composite, while the yield strength of the former is higher than that of the latter. Furthermore, the yield stress and tensile strength of Al_2O_3/Al nanocomposites increase with increasing alumina content up to 4 vol% at the expense of tensile ductility. For the nanocomposites with Al_2O_3 content ≥ 4 vol%, the strengthening effect levels off due to the agglomeration of alumina nanoparticles (Figure 8.14B). The main strengthening mechanism in the Al_2O_3/Al nanocomposites derives from the Orowan effect. However, agglomeration of alumina nanoparticles reduces Orowan strengthening when the alumina content ≥ 4 vol%.

Kollo et al. [44] fabricated n-SiC/Al nanocomposites using planetary milling process followed by hot extrusion. Figure 8.25 shows tensile stress−strain curves of pure Al and n-SiC/Al nanocomposites. Apparently, an addition of 1 vol% n-SiC to pure Al enhances its ultimate tensile strength from 100 to 205 MPa, being a twofold increment. At 10 vol% n-SiC, the tensile strength reaches 405 MPa with a

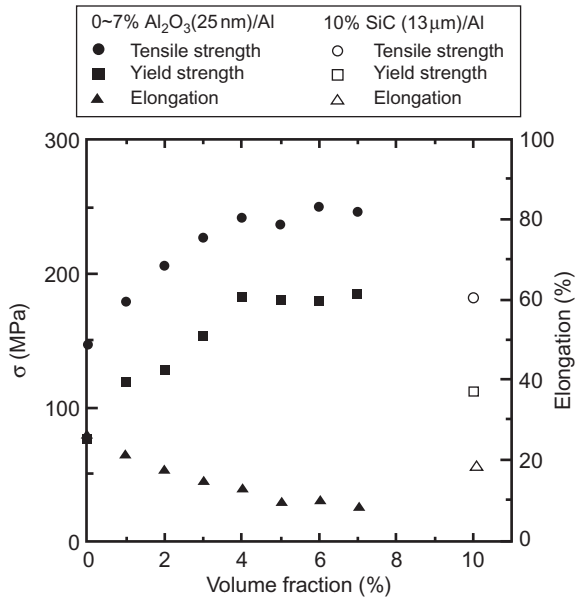

Figure 8.24 Tensile properties of PM-processed Al_2O_3/Al nanocomposites.
Source: Reprinted from Ref. [35] with permission of Elsevier.

drastic reduction in tensile ductility. More recently, Mobasherpour et al. [54] ball milled AA7075 alloy ((5.1−6.3 wt%)Zn−(2.1−2.9 wt%)Mg−(1.2−2 wt%)Cu and balance Al) with alumina nanoparticles. They reported that the hardness and ultimate tensile strength of Al_2O_3/AA7075 nanocomposites increase with increasing alumina content at the expense of tensile ductility.

For FSPed Al_2O_3/AA5052 composite specimens, alumina nanoparticles can disperse more uniformly in the alloy matrix by increasing the number of FSP passes as shown in Figure 8.26A and B[46]. The nominal composition of AA5052 alloy is 2.5 wt% Mg, 0.15 wt% Cr, 0.1 wt% Mn, 0.25 wt% Si, and 0.1 wt% Fe. The respective tensile strength, yield stress, and elongation of FSPed Al_2O_3/AA5052

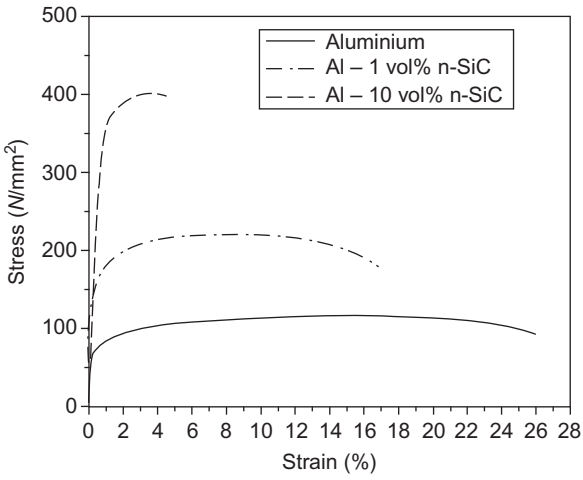

Figure 8.25 Tensile stress−strain curves of extruded Al and n-SiC/Al nanocomposites.
Source: Reprinted from Ref. [44] with permission of Elsevier.

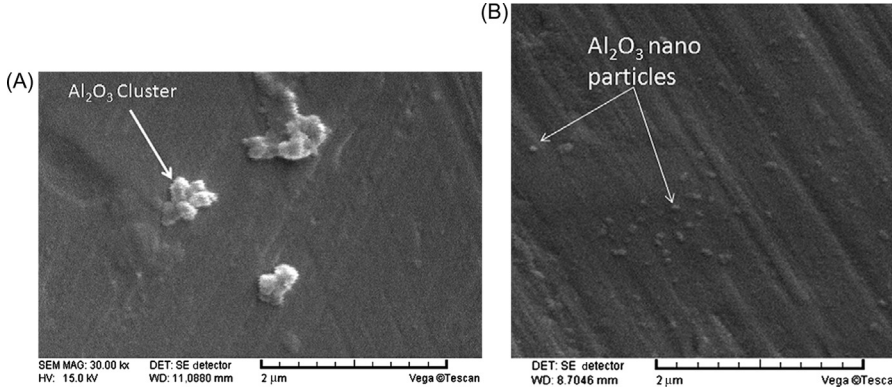

Figure 8.26 SEM micrograph of stir zone of the composite processed after (A) one pass and (B) four passes.
Source: Reprinted from Ref. [46] with permission of Elsevier.

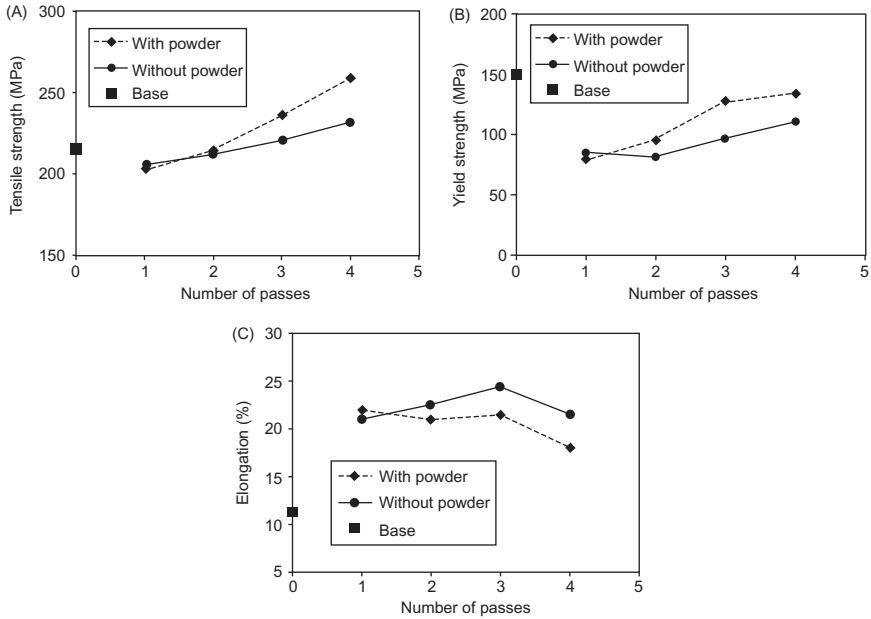

Figure 8.27 (A) Tensile strength, (B) yield strength, and (C) elongation as a function of number of passes for FSPed AA5052 alloy and Al_2O_3/AA5052 composite.
Source: Reprinted from Ref. [46] with permission of Elsevier.

specimens as a function of number of passes are shown in Figure 8.27A–C. Apparently, tensile and yield strengths of the composite specimens improve with increasing FSP passes because higher passes refine the matrix grain size in the stir processing zone effectively. Table 8.3 lists the tensile properties of PM aluminum-based nanocomposites.

8.3.2 Mg-Based Nanocomposites

8.3.2.1 Nanocomposites Fabricated by Liquid-State Processing

Li and coworkers fabricated Mg-based MMNCs reinforced with AlN or SiC nanoparticles using ultrasonic cavitation method [13,14,25,26]. Figure 8.28A and B shows typical tensile properties of AZ91D and 1 wt% AlN/AZ91D nanocomposite at room temperature and 200°C, respectively. At room temperature, the yield stress of AZ91D alloy and 1 wt% AlN/AZ91D nanocomposite is 100 and 144 MPa, respectively. The yield stress and tensile strength of AZ91D are enhanced by 44% and 18%, respectively, due to the AlN addition. The mechanical properties of 1 wt % AlN/AZ91D nanocomposite at 200°C are also improved. The yield stress of AZ91D is 87 MPa but increases to 105 MPa by adding 1 wt% AlN. The levels of enhancement in yield stress and tensile strength at 200°C are ~21% and 25%, respectively. The ductility of the 1 wt% AlN/AZ91D nanocomposite is improved

Table 8.3 Tensile Properties of PM Aluminum Matrix Nanocomposites

Particle Content (vol %)	Reinforcing Nanoparticle	Matrix Material	Fabrication Process	Yield Strength (MPa)	Tensile Strength (MPa)	Fracture Strain (%)	References
0	–	Al	PM process	68	103	–	[10]
1	Si_3N_4	Al	Dry powder mixing, hot pressing at 600°C, and hot extrusion at 420°C	144	180	17.4	[10]
0	–	Al	PM process	76	150	26	[35]
1.5	Al_2O_3	Al	Wet powder mixing in ethanol, cold isostatic pressing and sintering at 620°C for 2 h	124	176	21	[35]
0	–	Al	PM process	–	100	26	[44]
1	SiC	Al	MA followed by hot extrusion	–	205	17	[44]
10	SiC	Al	As above	–	405	4	[44]
0	–	AA7075	PM process	–	276	9	[54]
1	Al_2O_3	AA7075	MA followed by hot pressing at 450°C	–	317	3.2	[54]
3	Al_2O_3	AA7075	As above	–	365	3.1	[54]
5	Al_2O_3	AA7075	As above	–	443	2.1	[54]

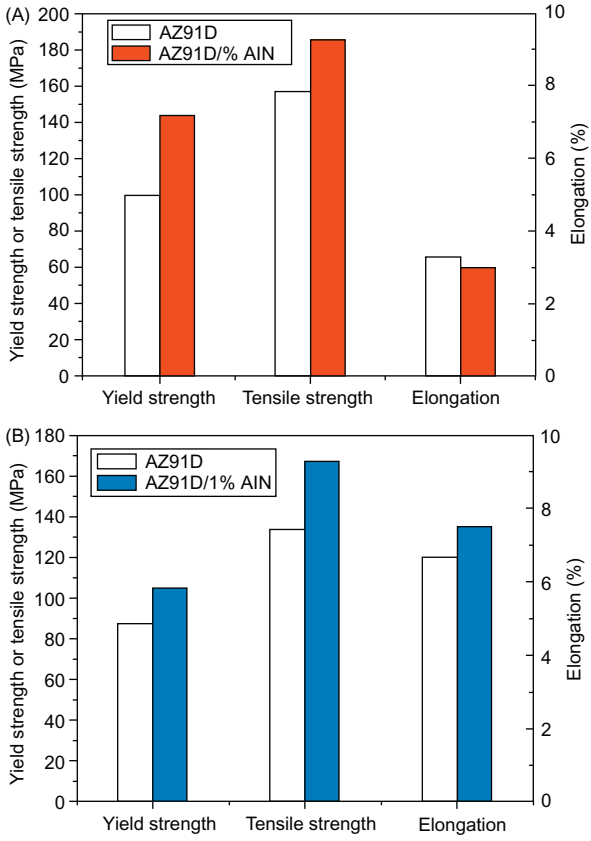

Figure 8.28 Tensile properties of AZ91D and 1 wt% AlN/AZ91D nanocomposite at (A) room temperature and (B) 200°C.
Source: Reprinted from Ref. [14] with permission of Elsevier.

slightly at 200°C. They reported that ultrasonic cavitation-based solidification processing is very efficient in dispersing AlN nanoparticles in magnesium melt. These well-dispersed nanoparticles improve the mechanical properties of nanocomposites significantly through the Orowan strengthening mechanism.

In the case of SiC/Mg nanocomposites, the incorporation of SiC nanoparticles into the Mg matrix refines its grain size markedly. However, some SiC microclusters still exist in the microstructures, especially at the grain boundaries [25,26]. Nevertheless, the addition of only 1 wt% SiC to magnesium increases its yield strength from 47 to 67 MPa [26]. From Eqs. (8.8)–(8.10), the yield stress of the composite (σ_{yc}) due to the Orowan strengthening, dislocation generation, and load-bearing effects is estimated to be 65 MPa, assuming $\sigma_{ym} = 47$ MPa, $d_p = 66$ nm, $G_m = (E_m/[2(1+\nu)]) = 16.5$ GPa, E_m (elastic modulus of Mg) = 42.8 GPa, ν (Poisson'ratio) = 0.3, $T_{process} = 750°C$, $T_{test} = 20°C$, $\alpha_m = 25 \times 10^{-6}$ $(°C)^{-1}$, $\alpha_p = 3.2 \times 10^{-6}$ $(°C)^{-1}$, and $b = 0.32$ nm. By further taking the Hall–Petch effect (Eq. (8.5)) into consideration, theoretical σ_{yc} value increases to 77 MPa. This predicted yield stress is somewhat larger than experimental yield stress of the nanocomposite, i.e., 67 MPa. This is due to the presence of SiC clusters in the

nanocomposite. Agglomeration of nanoparticles reduces the effect of Orowan mechanism by changing the effective distance between nanoparticles and the nature of the obstacles.

Nie et al. [27] utilized ultrasonic vibration during stir casting to fabricate 1 vol% SiC/AZ91 nanocomposite. In the process, SiC nanoparticles (60 nm) were added to molten magnesium alloy at 700°C under ultrasonic vibration for 20 min followed by casting into a mold. Most SiC nanoparticles are well dispersed in the matrix, with the presence of some SiC microclusters. The ultimate tensile strength, yield strength, and elongation to fracture of the 1 vol% SiC/AZ91 nanocomposite are considerably enhanced compared with those of the AZ91 alloy (Table 8.4). In another study, Nie et al. [28] produced compocast 1 vol% SiC/AZ91 nanocomposite assisted with ultrasonic vibration as shown in Figure 8.12. The formation of SiC nanoparticle clusters at the alloy grain boundaries was also observed. However, SiC nanoparticles disperse more uniformly within the alloy grains (Figure 8.29). The ultimate tensile strength, yield strength, and elongation to fracture of 1 vol% SiC/AZ91 nanocomposite stirring for 5 min are markedly improved compared with those of cast AZ91 alloy. However, the ultimate tensile strength and elongation to fracture of the 1 vol% SiC/AZ91 nanocomposite decreases with increasing the stirring time (Figure 8.30).

Gupta and coworkers investigated mechanical behavior of magnesium-based composites reinforced with alumina nanoparticles fabricated by DMD and hot extrusion processes technique [29–33]. Representative results of their studies are listed in Table 8.4. It appears that small additions of alumina nanoparticles to pure magnesium and AZ31 alloy increase the yield stress, tensile strength, and tensile ductility considerably. It is noted that the tensile ductility of magnesium and AZ31 alloy improves greatly by incorporating alumina nanoparticles in their lattices. The improvement in tensile ductility of Mg-based nanocomposites is attributed to the activation of the basal slip system by ceramic nanoparticles. Magnesium generally exhibits low tensile ductility because of its HCP structure having three independent slip system only. In this regard, basal slip is difficult for pure Mg during mechanical deformation at room temperature. However, alumina nanoparticles in the magnesium matrix tends to activate basal slip during tension, leading to enhanced tensile ductility. Table 8.4 summarizes tensile properties of the Mg-based MMNCs prepared by liquid metallurgy route.

8.3.2.2 Nanocomposites Fabricated by Solid-State Processing

Gupta and coworkers also fabricated 1.1 vol% Al_2O_3/Mg nanocomposite using simple powder mixing and sintering [30]. Their results demonstrated that alumina nanoparticle addition increases the yield stress, tensile strength, and tensile ductility of magnesium. Similarly, low volume fractions of SiC nanoparticles are also beneficial in enhancing mechanical properties of magnesium nanocomposites fabricated by means of microwave sintering [47]. On the contrary, Ferkel and Mordike [48] indicated that the room temperature tensile strength of extruded 3 vol% SiC/Mg nanocomposite prepared by simple powder mixing is poorer than that of

Table 8.4 Tensile Properties of Cast Magnesium Matrix Nanocomposites

Particle Content (vol %)	Particle Content (wt %)	Nanoparticle	Matrix Material	Fabrication Process	Yield Strength (MPa)	Tensile Strength (MPa)	Fracture Strain (%)	References
–	0	–	AZ91D	Melt casting	100	160	3.3	[14]
–	1	AlN	AZ91D	Melting at 700°C assisted with ultrasonic vibration	144	187	3.0	[14]
–	0	–	Pure Mg	Melt casting	47	120	12.3	[26]
–	1	SiC	Pure Mg	Melting at 750°C assisted with ultrasonic vibration	67	133	6.3	[26]
0	–	–	Pure Mg	DMD and hot extrusion	97	173	7.4	[29]
0.22	0.5	Al_2O_3	Pure Mg	As above	146	207	8.0	[29]
0.66	1.5	Al_2O_3	Pure Mg	As above	170	229	12.4	[29]
1.11	2.5	Al_2O_3	Pure Mg	As above	175	246	14.0	[29]
–	–	Al_2O_3	AZ31	As above	172	263	10.4	[31]
–	1.5	Al_2O_3	AZ31	As above	204	317	22.2	[31]
–	0	–	Mg−2Al−1Si	Melt casting	48.6	137.9	9.2	[25]
–	2	SiC	Mg−2Al−1Si	Melting at 700°C assisted with ultrasonic vibration	73.8	157.2	7.5	[25]
–	0	–	Mg−4Al−1Si	As above	61.9	144.8	8.8	[25]
–	2	SiC	Mg−4Al−1Si	As above	82.1	177.9	9.5	[25]
0	–	–	AZ91	Casting without sonic probe	72	125	2	[27]
1	–	SiC	AZ91	Stir casting at 700°C assisted with ultrasonic vibration	90	220	8	[27]
1	–	SiC	AZ91	Compocasting assisted with ultrasonic vibration	88	188	5.5	[28]

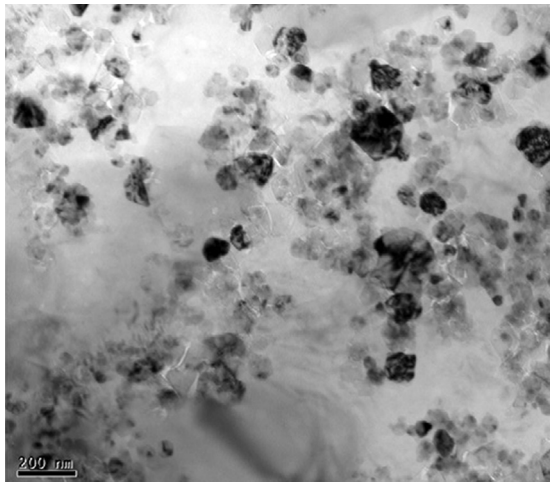

Figure 8.29 TEM image of 1 vol % SiC/AZ91 nanocomposite showing local dispersion of SiC nanoparticles.
Source: Reprinted from Ref. [28] with permission of Elsevier.

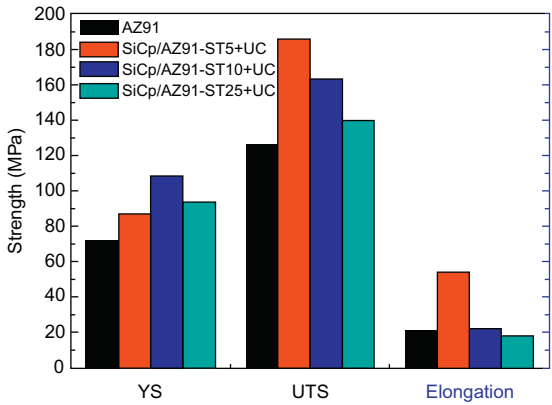

Figure 8.30 Tensile properties compocast AZ91 and 1 vol% SiC/AZ91 nanocomposite. ST5, ST10, and ST25 imply stirring liquid melt for 5, 10, and 25 min, respectively. UC implies ultrasonic cavitation.
Source: Reprinted from Ref. [28] with permission of Elsevier.

extruded Mg. This is due to nonuniform dispersion of SiC nanoparticles in the Mg matrix. However, the room temperature tensile strength of extruded 3 vol% SiC/Mg nanocomposite prepared by ball milling is much higher than that of extruded Mg (Figure 8.31A). At 100°C, SiC nanoparticles are beneficial to enhance its tensile strength due to the softening of the Mg matrix (Figure 8.31B).

Lee et al. [55] employed FSP to disperse SiO_2 nanoparticles (20 nm) in the AZ61 alloy having a nominal composition of Mg−6.02% Al−1.01% Zn−0.30% Mn. Silica nanoparticles are uniformly dispersed in surface alloy matrix after four FSP passes. The tensile properties of AZ61, FSP-processed AZ61 and its nanocomposites are tabulated in Table 8.5. The yield stress and tensile strength of FSPed SiO_2/AZ61 nanocomposites are considerably higher than those of pristine AZ61 and FSP-processed AZ61 as expected (Table 8.5). Furthermore, FSP treatment reduces the grain size of pristine AZ61 alloy markedly from 75 μm down to

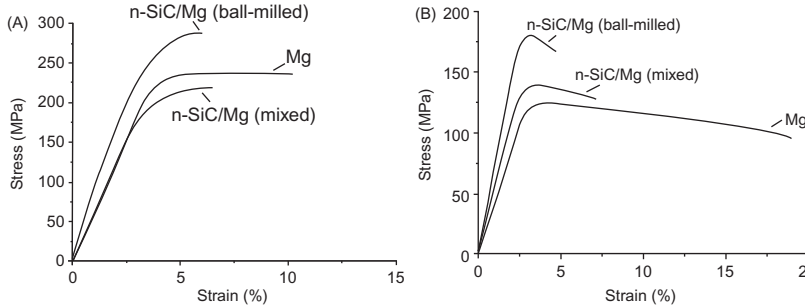

Figure 8.31 Stress–strain curves of extruded Mg and extruded 3 vol% SiC/Mg nanocomposite specimens prepared by powder mixing or ball milling at (A) room temperature and (B) 100°C.
Source: Reprinted from Ref. [48] with permission of Elsevier.

7–8 μm via dynamic recrystallization. This leads to improved yield stress and tensile strength of the alloy. Finally, FSP method is an effective secondary mechanical treatment to remove internal defects of cast magnesium alloy [38,49]. For example, FSP can dissolve hard β-$Mg_{17}Al_{12}$ phase in the grain boundaries of cast AZ91 alloy. This phase often acts as the favorable site for the crack nucleation. Moreover, porosities and voids that reduce tensile strength and elongation of the cast AZ91 alloy are also eliminated by the FSP treatment. Therefore, the resulting nanocomposites exhibit higher tensile ductility than the cast alloy (Table 8.5).

8.4 Conclusions

Ceramic nanoparticles are attractive reinforcing materials for metals to form MMNCs of high mechanical strength and stiffness for structural engineering applications. The mechanical performance of MMNCs depends greatly on the attainment of homogeneous dispersion of ceramic nanoparticles in the metal matrix. Ceramic nanoparticles of large surface-to-volume ratio are poorly wetted with metals, thus causing the formation of particle clusters in the metal matrix. As a result, the resulting nanocomposites exhibit poor mechanical properties.

Liquid-state processing route can manufacture MMNCs in large quantities at a relatively low cost using existing melting and casting equipments. However, ceramic nanoparticles pose serious difficulty in achieving a uniform dispersion because of their high viscosity in molten melt and poor wettability. In this regard, compocasting and ultrasonic vibration are effective techniques to disperse ceramic nanoparticles in molten metal or semisolid metal. PM route can manufacture dense

Table 8.5 Tensile Properties of Magnesium Matrix Nanocomposites Fabricated by Solid-State Processing Route

Particle Content (vol %)	Particle Content (wt %)	Nanoparticle	Matrix Material	Fabrication Process	Yield Strength (MPa)	Tensile Strength (MPa)	Fracture Strain (%)	References
–	0	–	Pure Mg	Dry powder mixing and sintering	132	193	4.2	[30]
0.66	1.5	Al_2O_3	Pure Mg	As above	194	250	6.9	[30]
–	0	–	Pure Mg	Dry powder mixing and microwave sintering	125	172	5.8	[47]
–	0.35	SiC	Pure Mg	As above	132	194	6.3	[47]
–	0.5	SiC	Pure Mg	As above	144	194	7.0	[47]
–	1.0	SiC	Pure Mg	As above	157	403	7.6	[47]
0	–	–	AZ61	Billet alloy	140	190	13	[55]
0	–	–	AZ61	Four FSP passes	147	242	11	[55]
5	–	SiO_2	AZ61	Two FSP passes	185	219	10	[55]
5	–	SiO_2	AZ61	Four FSP passes	214	233	8	[55]
10	–	SiO_2	AZ61	Two FSP passes	200	246	4	[55]
10	–	SiO_2	AZ61	Four FSP passes	225	251	4	[55]
0	–	–	AZ91	Cast alloy	–	139	6.74	[38]
8	–	SiO_2	AZ91	One FSP pass	–	193	12.56	[38]
8	–	SiO_2	AZ91	Two FSP passes	–	233	13.42	[38]
8	–	SiO_2	AZ91	Three FSP passes	–	279	14.67	[38]

MMNCs of higher tensile strength and ductility than the casting process. The high cost of powder materials restricts its use for manufacturing nanocomposite structural components in the industrial sectors.

References

[1] Dragone TL, Nix WD. Steady state and transient creep properties of an aluminum alloy reinforced with alumina fibers. Acta Metall Mater 1992;40(10):2781–91.

[2] Tjong SC, Mai YW. Processing structure–property aspects of particulate- and whisker-reinforced titanium matrix composites. Compos Sci Technol 2008;68 (3–4):583–601.

[3] Ma ZY, Mishra RS, Tjong SC. High-temperature creep behavior of TiC particulate reinforced Ti–6Al–4V alloy composite. Acta Mater 2002;50(17):4293–302.

[4] Ma ZY, Tjong SC. Microstructural and mechanical characteristics of *in situ* metal matrix composites. Mater Sci Eng R 2000;29(3–4):49–113.

[5] Tjong SC, Lau KC. Abrasive wear behavior of TiB_2 particle-reinforced copper matrix composites. Mater Sci Eng A 2000;282(1–2):183–6.

[6] Tjong SC, Lau KC. Properties and abrasive wear of TiB2/Al–4% Cu composites produced by hot isostatic pressing. Compos Sci Technol 1999;59(13):2005–13.

[7] Rawal J. Metal–matrix composites for space applications. JOM 2001;53(4):14–7.

[8] Micracle DB. Metal matrix composites—from science to technological significance. Compos Sci Technol 2005;65:2526–40.

[9] Tjong SC, Chen H. Nanocrystalline materials and coatings. Mater Sci Eng R 2004;45 (1–2):1–88.

[10] Ma ZY, Li YL, Liang Y, Zheng F, Bi J, Tjong SC. Nanometric Si_3N_4 particulate-reinforced aluminum composite. Mater Sci Eng A 1996;219(1–2):229–31.

[11] Ma ZY, Tjong SC, Li YL, Liang Y. High temperature creep behavior of nanometric Si_3N_4 particulate reinforced aluminium composite. Mater Sci Eng A 1997;225 (1–2):125–34.

[12] Yang Y, Lan J, Li XC. Study of bulk aluminum matrix nanocomposite fabricated by ultrasonic dispersion of nanosized SiC particles in molten aluminum alloy. Mater Sci Eng A 2004;380(1–2):378–83.

[13] Lan J, Yang Y, Li XC. Microstructure and microhardness of SiC nanoparticles reinforced magnesium composites fabricated by ultrasonic method. Mater Sci Eng A 2004;386(1–2):284–90.

[14] Cao G, Choi H, Oportus J, Konishi H, Li XC. Study on tensile properties and microstructure of cast AZ91D/AlN nanocomposites. Mater Sci Eng A 2008;494 (1–2):127–31.

[15] Wang D, De Cicco MP, Li XC. Using diluted master nanocomposites to achieve grain refinement and mechanical property enhancement in as cast Al–9Mg alloy. Mater Sci Eng A 2012;532:396–400.

[16] Su H, Gao W, Feng Z, Lu Z. Processing, microstructure and tensile properties of nanosized Al_2O_3 particle reinforced aluminum matrix composites. Mater Des 2012;36:590–6.

[17] Schultz BF, Ferguson JB, Rohatgi PK. Microstructure and hardness of Al_2O_3 nanoparticle reinforced Al–Mg composites fabricated by reactive wetting and stir mixing. Mater Sci Eng A 2011;530:87–97.

[18] Tahamtan S, Halvaee A, Emamy M, Zabihi MS. Fabrication of Al/A206−Al_2O_3 nano/micro composite by combining ball milling and stir casting technology. Mater Des 2013;49:347−59.
[19] Sajjadi SA, Ezatpour HR, Parizi MT. Comparison of microstructure and mechanical properties of A356 aluminum alloy/Al_2O_3 composites fabricated by stir and compocasting processes. Mater Des 2012;34:106−11.
[20] Selvam JD, Smart DS, Dinaharan I. Microstructure and some mechanical properties of fly ash particulate reinforced AA6061 aluminum alloy composites prepared by compocasting. Mater Des 2013;49:28−34.
[21] Sajjadi SA, Parizi MT, Ezatpour HR, Sedghi A. Fabrication of A356 composite reinforced with micro and nanoAl_2O_3 particles by a developed compocasting method and study of its properties. J Alloys Compd 2012;511(1):226−31.
[22] Mazahery A, Abdizadeh H, Baharvandi HR. Development of high performance A356/nano-Al_2O_3 composites. Mater Sci Eng A 2009;518(1−2):61−4.
[23] El-Mahallawi I, Abdelkader H, Yousef L, Amer A, Mayer J, Schwedt A. Influence of Al_2O_3 nano-dispersions on microstructure features and mechanical properties of cast and T6 heat-treated AlSi hypoeutectic Alloys. Mater Sci Eng A 2012;556:76−87.
[24] Mordike BL, Ebert T. Magnesium: properties−applications−potential. Mater Sci Eng A 2002;302(1):37−45.
[25] Cao G, Konishi H, Li XC. Mechanical properties and microstructure of SiC-reinforced Mg-(2,4)Al−1Si nanocomposites fabricated by ultrasonic cavitation based solidification processing. Mater Sci Eng A 2008;486(1−2):357−62.
[26] Erman A, Groza J, Li XC, Choi H, Cao G. Nanoparticle effects in cast Mg−1 wt% SiC nanocomposites. Mater Sci Eng A 2012;558:39−43.
[27] Nie KB, Wang XJ, Hu XS, Xu L, Wu K, Zheng MY. Microstructure and mechanical properties of SiC nanoparticles reinforced magnesium matrix composites by ultrasonic vibration. Mater Sci Eng A 2011;528(15):5278−82.
[28] Nie KB, Wang XJ, Wu K, Xu L, Zheng MY, Hu XS. Processing, microstructure and mechanical properties of magnesium matrix nanocomposites fabricated by semisolid stirring assisted ultrasonic vibration. J Alloys Compd 2011;509(35):8664−9.
[29] Hassan SF, Gupta M. Development of high performance magnesium nanocomposites using solidification processing route. Mater Sci Technol 2005;20(11):1383−8.
[30] Hassan SF, Gupta M. Effect of type of primary processing on the microstructure, CTE and mechanical properties of magnesium/alumina nanocomposites. Comp Struct 2006;72(1):19−26.
[31] Paramsothy M, Hassan SF, Srikanth N, Gupta M. Enhancing tensile/compressive response of magnesium alloy AZ31 by integrating with Al_2O_3 nanoparticles. Mater Sci Eng A 2009;527(1−2):162−8.
[32] Paramsothy M, Nguyen QB, Tun KS, Chan J, Kwok R, Kuma JV, et al. Mechanical property retention in remelted microparticle to nanoparticle AZ31/Al_2O_3 composites. J Alloys Compd 2010;506(2):600−6.
[33] Hassan SF, Paramsothy M, Patel F, Gupta M. High temperature tensile response of nano-Al_2O_2 reinforced AZ31 nanocomposites. Mater Sci Eng A 2012;558:278−84.
[34] Ho KF, Gupta M, Srivatsan TS. The mechanical behavior of magnesium alloy AZ91 reinforced with fine copper particulates. Mater Sci Eng A 2004;369(1−2):302−8.
[35] Kang YC, Chan SL. Tensile properties of nanometric Al_2O_3 particulate-reinforced aluminum matrix composites. Mater Chem Phys 2004;85(2−3):438−43.
[36] Suryanarayana C, Al-Aqeeli N. Mechanically alloyed nanocomposites. Prog Mater Sci 2013;58(4):383−502.

[37] Mishra RS, Ma ZY. Friction stir welding and processing. Mater Sci Eng R 2005;50 (1–2):1–78.
[38] Khayyamin D, Mostafapour A, Keshmiri R. The effect of process parameters on microstructural characteristics of AZ91/SiO_2 composite fabricated by FSP. Mater Sci Eng A 2013;559:217–21.
[39] Bauri R, Yadav D, Suhas G. Effect of friction stir processing on microstructure and properties of Al-TiC *in situ* composite. Mater Sci Eng A 2011;528(13–14):4732–9.
[40] Razavi Hesabi Z, Simchi A, Seyed Reihani SM. Structural evolution during mechanical milling of nanometric and micrometric Al_2O_3 reinforced Al matrix composites. Mater Sci Eng A 2006;428(1–2):159–68.
[41] Zebarjad SM, Sajjadi SA. Microstructure evaluation of Al–Al_2O_3 composite produced by mechanical alloying method. Mater Des 2006;27(8):684–8.
[42] Zebarjad SM, Sajjadi SA. Dependency of physical and mechanical properties of mechanical alloyed Al–Al_2O_3 composite on milling time. Mater Des 2007;28 (7):2113–20.
[43] Bathula S, Anandani RC, Dhar A, Srivastava AK. Microstructural features and mechanical properties of Al 5083/SiCp metal matrix nanocomposites produced by high energy ball milling and spark plasma sintering. Mater Sci Eng A 2012;545:97–102.
[44] Kollo L, Bradbury CR, Veinthal R, Jaggi C, Carreno-Morelli E, Leparoux M. Nano-silicon carbide reinforced aluminium produced by high-energy milling and hot consolidation. Mater Sci Eng A 2011;528(21):6606–15.
[45] Shafiei-Zarghani A, Kashani-Bozorg SF, Zarei-Hanzaki A. Microstructures and mechanical properties of Al/Al_2O_3 surface nanocomposite layer produced by friction stir processing. Mater Sci Eng A 2009;500(1–2):84–91.
[46] Sharifitabar M, Sarani A, Khorshahian S, Shafiee Afarani M. Fabrication of 5052 AlAl_2O_3 ceramic particle reinforced composite via friction stir processing route. Mater Des 2011;32(8–9):4164–72.
[47] Wong WL, Gupta M. Simultaneously improving strength and ductility of magnesium using nano-size SiC particulates and microwaves. Adv Eng Mater 2006;8(8):735–9.
[48] Ferkel H, Mordike BL. Magnesium strengthened by SiC nanoparticles. Mater Sci Eng A 2001;298(1–2):193–9.
[49] Faraji G, Asad P. Characterization of AZ91/alumina nanocomposite produced by FSP. Mater Sci Eng A 2011;528(6):2431–40.
[50] Dieter GE. Mechanical metallurgy. 3rd ed. New York: McGraw-Hill; 1988. p. 212–20.
[51] Clyne TW, Withers PJ. An introduction to metal matrix composites. Cambridge: University Press; 1993.
[52] Zhang Z, Chen DL. Consideration of Orowan strengthening effect in particulate reinforced metal matrix nanocomposites: a model for predicting their yield strength. Scripta Mater 2006;54(7):1321–6.
[53] Karbalaei Akbari M, Mirzaee O, Baharvandi HR. Fabrication and study on mechanical properties and fracture behavior of nanometric Al_2O_3 particle-reinforced A356 composites focusing on the parameters of vortex method. Mater Des 2013;46:199–205.
[54] Mobasherpour I, Tofigh AA, Ebrahimi M. Effect of nano-size Al_2O_3 reinforcement on the mechanical behavior of synthesis 7075 aluminum alloy composites by mechanical alloying. Mater Chem Phys 2013;138(2–3):535–41.
[55] Lee CJ, Huang JC, Hsieh PJ. Mg based nanocomposites fabricated by friction stir processing. Scripta Mater 2006;54(7):1415–20.